CrystEngComm

ROYAL SOCIETY OF CHEMISTRY

PAPER

View Article Online
View Journal | View Issue

Cite this: *CrystEngComm*, 2022, **24**, 543

A triphenylamine derivative and its Cd(II) complex with high-contrast mechanochromic luminescence and vapochromism†

Qiong-Fang Liang, Han-Wen Zheng, Dong-Dong Yang and Xiang-Jun Zheng *

An acetonitrile solvate of a Schiff base molecule (HL) with acetonitrile (**HL**·2CH_3CN) and its Cd(II) complex ($Cd(HL)_2Cl_2$, **1**) was designed and synthesized. The different conformation of HL in **HL**·2CH_3CN is adjusted by the hydrogen bonding O–H···O between HL molecules, together with N–H···N between HL molecules and acetonitrile molecules. Meanwhile, the conformation of HL in complex **1** is adjusted by coordination interactions between Zn ions and atoms O and N, together with hydrogen bonding N–H···Cl. The presence of the triphenylamine group makes **HL**·2CH_3CN and complex **1** loosely packed. Upon grinding, **HL**·2CH_3CN and complex **1** both showed high-contrast mechanochromic luminescence (MCL) change from blue to green and cyan to yellow, respectively. These changes can be eliminated by fumigation with organic vapor. The results of powder X-ray diffraction (PXRD) show that their MCL is due to the phase transformation from a crystalline state to an amorphous state. In addition, **HL**·2CH_3CN and complex **1** also exhibited high-contrast acidochromism upon exposure to HCl and NH_3 vapor. X-ray photoelectron spectroscopy (XPS) and PXRD studies show that the protonation of the –NH– group together with phase transformation from a crystalline state to an amorphous state is attributed to the fluorescence switching. For **HL**·2CH_3CN, the protonation process was accompanied by the departure of acetonitrile molecules. The emission of **HL** was restored to the amorphous state rather than the original crystalline state emission after further exposure to NH_3 vapor, while **1**-**HCl** could revert to the original crystalline state emission. In addition, **HL**·2CH_3CN and complex **1** have been successfully used to produce writable and acid-responsive test papers.

Received 29th September 2021,
Accepted 25th November 2021

DOI: 10.1039/d1ce01319j

rsc.li/crystengcomm

Introduction

Stimulus responsive luminescent materials can reversibly change their luminescence in response to external stimuli (such as mechanical stress, chemical vapor, light, and heat).[1–10] The high-contrast luminescence color or intensity change can be easily observed by the naked eye, making them good candidate materials in the fields of chemical sensors, environmental monitoring, data recording, optoelectronic devices, and security inks.[11–22] Among them, mechanical force is one of the most common stimuli in nature. Therefore, mechanochromic luminescent (MCL) materials that can change their luminescence characteristics when exposed to external mechanical forces (such as shearing, scratching, grinding, and crushing) have attracted extensive attention. The original emission states can be restored by applying another external stimulus (such as chemical vapor or heat) to achieve reversible mechanochromic luminescence.[23–30] In recent years, there have been many reports on MCL materials including organic molecules,[31,32] metal–organic complexes,[30,33,34] and organic polymers.[35,36] Currently, the mechanism of the mechanochromic behavior is mainly attributed to the phase transformation from a crystalline state to an amorphous state or single-crystal-to-single-crystal transformation.[37–40] Hydrogen bonding, π–π stacking, metal–metal interaction and other intermolecular interactions as the driving forces for molecular arrangement and packing can be changed when exposed to external stimuli, so that the molecular packing mode and conformation are changed and the HOMO–LUMO energy levels are perturbed, consequently resulting in the MCL properties.[28,41–44] Therefore, designing a distorted molecule with loose molecular packing modes, making the intermolecular interactions easily damaged or modified by external mechanical stimuli, is a convenient and effective strategy to achieve MCL. It has been proved workable by adopting D–A structure, introducing rotatable aromatic ring and flexible group.[1,6,12,13,23,37,38,40,44–46] For vapochromic

Beijing Key Laboratory of Energy Conversion and Storage Materials, College of Chemistry, Beijing Normal University, Beijing 100875, P. R. China.
E-mail: xjzheng@bnu.edu.cn

† Electronic supplementary information (ESI) available: Tables S1 and S2 and Fig. S1–S9 (PDF) showing the structures, spectra, TGA curves, DSC curves, dihedral angles, and X-ray crystallographic data for **HL**·2CH_3CN and complex **1** (CIF). CCDC 2099606 and 2099607. For ESI and crystallographic data in CIF or other electronic format see DOI: 10.1039/d1ce01319j

luminescence materials, their color or emission can change reversibly when exposed to the vapor atmosphere of volatile compounds.[47] Generally, conformational changes, proton transfer, changes in intermolecular interactions, and the adsorption and desorption of vapor molecules are referred as the mechanism of this process.[4,5,16–18,48,49] Among them, quite a few materials have been exploited for demonstrating fluorescence switching by treating with HCl and NH_3 vapor.[50–52]

A triphenylamine (TPA) moiety is a typical electron donor with a propeller-shape non-coplanar structure, and is widely used in the fabrication of efficient luminescent solid materials due to its high photoelectric energy conversion efficiency and hole-transporting capability.[53–55] On the other hand, the highly distorted structure of the triphenylamine moiety prevents the formation of close molecular packing and produces loose aggregation patterns, which has also been applied in the design of stimulus-responsive smart luminescent materials.[56–60] Here, we designed and synthesized the Schiff base molecule **HL** and its Cd(II) complex with 4-(diphenylamino)benzaldehyde as the electron donor and 4-hydroxybenzohydrazide as the acceptor. The molecule HL contains rich hydrogen bond donors and acceptors, such as OH, NH, C=N and carbonyl groups, which could affect the molecular conformation through hydrogen bonding. **HL** could adopt a highly distorted structure and loose molecular packing mode. After the coordination with a Cd^{2+} ion, the conformation of the Schiff base molecule changes, and the emission position of the Cd complex is different from that of **HL**·$2CH_3CN$, indicating that the formation of coordination bonds and hydrogen bonds regulates the luminescence properties of the Schiff base molecule successfully. Both Schiff base ligands and their complexes exhibit high-contrast mechanochromic luminescence due to the phase transformation from the crystalline state to the amorphous state. More interestingly, color and emission changes were also observed after being exposed to hydrochloric acid vapor, indicating that **HL** and its Cd complex also have acid–base responsive properties.

Results and discussion

Crystal structure of HL·$2CH_3CN$ and complex 1

As shown in Scheme 1, both Schiff base **HL** and complex **1** are synthesized by a one-pot method through the aldimine condensation reaction.

Both **HL**·$2CH_3CN$ and complex **1** have the same crystal system (triclinic) and space group ($P\bar{1}$), but different stacking modes. As shown in Fig. 1a, there are two Schiff base molecules with different orientations and four acetonitrile molecules in the unit cell of **HL**·$2CH_3CN$, and the Schiff base molecules are highly staggered. There are a variety of intermolecular hydrogen bonds such as N–H···N (3.045–3.051 Å), O–H···O (2.670–2.737 Å), C–H···N (3.332–3.434 Å) and C–H···O (3.374 Å) in the crystal, as well as weak C–H···π (2.61–2.96 Å) interactions, which hold the Schiff base molecules and acetonitrile molecules together (Fig. S1†). It is worth noting that the Schiff base molecules are arranged in a staggered arrangement through the O–H···O hydrogen bonds formed by the carbonyl O atom and the phenolic hydroxyl group, and the Schiff base molecules and the acetonitrile molecules interact through the N–H···N hydrogen bonds formed by the N atom of the acetonitrile molecule and the –NH– group of the Schiff base molecule (Fig. 2a). For every HL molecule, there are four aromatic rings. For convenience, they are defined as rings A, B, C and D, respectively. These rings do not adopt a coplanar conformation, and there are large dihedral angles between them as expected (Table S1†). The dihedral angles of the different rings are in the range of 47.1–80.41°, indicating that the molecules are highly twisted.

For complex **1**, one cadmium ion is coordinated with two Schiff base ligands arranged head-to-tail and two chloride ions to form a six-coordination octahedral geometry. Due to the participation of chloride ions, the Schiff base ligands are not deprotonated but in neutral form. There are also a variety of intermolecular hydrogen bonds O–H···Cl (3.168 Å) (Fig. 2b) and intramolecular hydrogen bonds, such as N–H···Cl (3.307 Å), C–H···Cl (3.521–3.569 Å) and C–H···O (3.254–3.266 Å), and intermolecular C–H···π (2.800 Å) interactions in complex **1**. Due to the coordination with a Cd^{2+} ion, on the one hand, there is O–H···Cl hydrogen

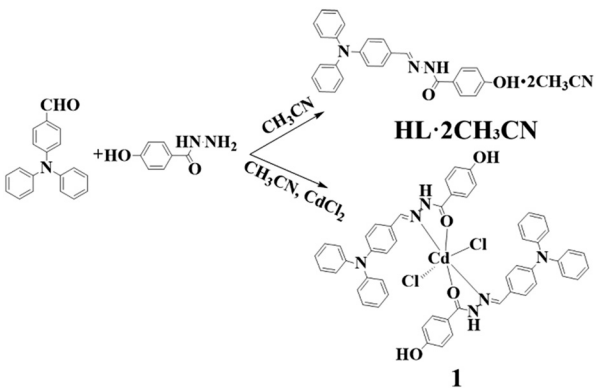

Scheme 1 Synthetic routes of HL·$2CH_3CN$ and complex **1**.

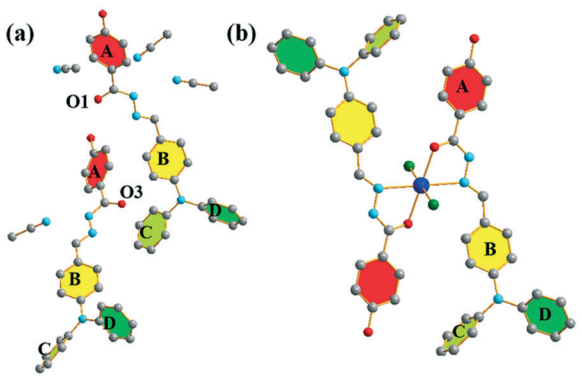

Fig. 1 Molecular structures of HL·$2CH_3CN$ (a) and complex **1** (b).

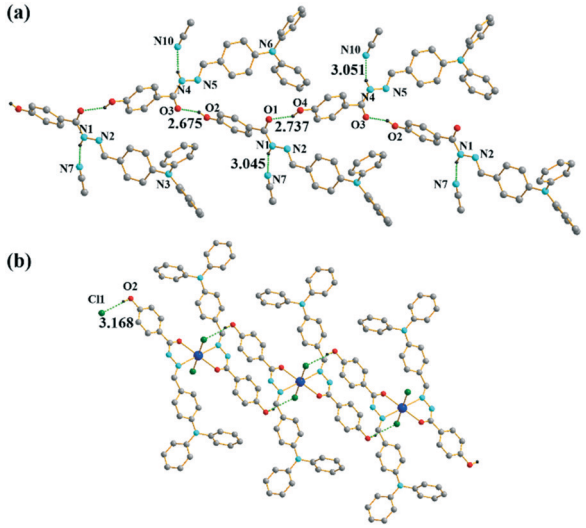

Fig. 2 Main intermolecular hydrogen bonding in HL·2CH_3CN (a) and complex **1** (b).

bonding between two adjacent coordination compounds, which is completely different from HL·2CH_3CN. On the other hand, there are π–π interactions (3.831–3.936 Å) between the aromatic rings of the triphenylamine moiety in complex **1**, which makes the molecule extend into a one-dimensional chain along the *a*-axis (Fig. S1†). In addition, the dihedral angle between rings A and B of the Schiff base molecule in complex **1** is only 12.05°, much smaller than that in HL·2CH_3CN, indicating that the Schiff base molecule in complex **1** has better planarity than that in HL·2CH_3CN. The dihedral angles between other rings are also different as shown in Table S1.† It is the different interactions, especially hydrogen bonding between the molecules, that result in the different molecular conformation for HL.

Mechanochromic luminescence properties

The crystals of HL·2CH_3CN showed blue fluorescence with an emission peak at 464 nm under the irradiation of a 365 nm UV lamp (Fig. 3a), with the fluorescence lifetime τ = 1.03 ns and Φ_F = 4.80% (Fig. S2†). Maybe due to the existence of acetonitrile molecules in the lattice, the crystals of HL·2CH_3-CN are apt to effloresce with the emission red-shifted to 483 nm as shown in Fig. 3c. After grinding with a pestle in a mortar, the fluorescence emission position red-shifted to 520 nm (τ = 1.36 ns, Φ_F = 4.60%), accompanied by the appearance of green fluorescence. When the ground sample was exposed to acetonitrile vapor, the emission peak returned to the original emission of 464 nm with the blue fluorescence observed again. But when the fumed sample was placed under ambient conditions for 10 minutes, the emission shifted to 473 nm. The MCL process was also observed in complex **1**. Under 365 nm UV lamp irradiation, complex **1** exhibited cyan emission with a peak at 490 nm, and with the fluorescence lifetime τ = 1.31 ns and Φ_F = 20.1% (Fig. S3†), indicating that the excited state energy level of the ligand was changed after coordination. After grinding, the emission peak red-shifted to 572 nm (τ = 3.27 ns, Φ_F = 14.8%), and the emission color changed to yellow. After fumigating the ground sample with ether, it can be observed that the luminous color returns to green, and the emission position returns to 538 nm (Fig. 3b and d). The changes of the emission colors of HL·2CH_3CN and complex **1** under different external mechanical stimuli were quantified with the CIE diagrams as shown in Fig. S4.† Therefore, both HL·2CH_3CN and complex **1** exhibited high-contrast MCL properties.

In order to investigate the MCL mechanisms of HL·2CH_3-CN and complex **1**, PXRD experiments on the samples in different states were carried out. It can be seen from Fig. 4a and b that the experimental spectrum of the original sample of HL·2CH_3CN is consistent with the PXRD pattern simulated by the single crystal data, indicating that the original sample has good crystallinity and purity. The disappearance of the diffraction peaks upon grinding indicated that grinding caused a phase transformation from a crystalline state to an amorphous state. In addition, comparing the thermogravimetric analysis (TGA) curve (Fig. S5†) of the original crystals with that of the ground sample of HL·2CH_3CN, the original crystal began to lose weight at 60 °C, which was attributed to the loss of acetonitrile molecules in the crystal lattice. Meanwhile, there is no weight loss for the ground sample at this temperature, indicating that grinding also led to the departure of acetonitrile molecules. In the PXRD pattern of the fumed sample, the diffraction peaks consistent with the original crystal did not all recover, which may be due to the efflorescence of the sample after

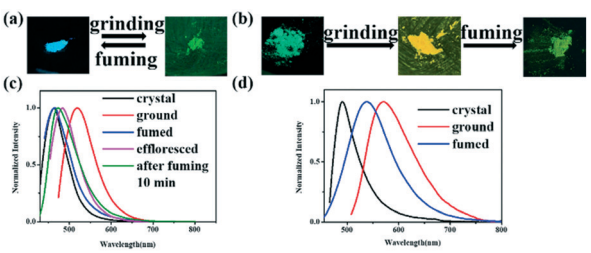

Fig. 3 Emission images of HL·2CH_3CN (a) and complex **1** (b) in different solid states under the irradiation of UV light at 365 nm. Emission spectra of HL·2CH_3CN (c) and complex **1** (d) in different solid states.

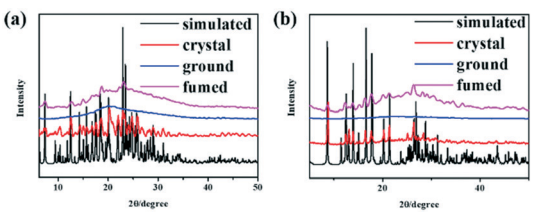

Fig. 4 PXRD patterns of HL·2CH_3CN (a) and complex **1** (b) in different states.

leaving the acetonitrile vapor atmosphere. The disappearance and recovery of the diffraction peaks can also be seen in the PXRD patterns of complex **1** in different states. Moreover, the diffraction pattern of the fumed sample showed that the sample is a mixture of the amorphous state and the original crystalline state, which is consistent with the redshift of the emission peak of the sample compared to that of the original sample. The transformation from the crystalline state to the amorphous state was further confirmed by differential scanning calorimetry (DSC) experiments. The ground sample of **HL**·2CH_3CN exhibited an exothermic peak at 200 °C upon heating, which originated from the cold recrystallization (Fig. S6†). Similar experimental results were also obtained with the ground sample of complex **1**. These experimental results showed that the high-contrast MCL processes of complex **1** and **HL**·2CH_3CN were due to the phase transformation from the crystalline state to the amorphous state, while the high-contrast process of **HL**·2CH_3CN was also accompanied by the departure and recovery of the acetonitrile molecules. As mentioned above, the existence of weak interactions and the dihedral angles between the rotatable aromatic rings makes the molecules adopt a loose and easily-destructible packing mode. Upon grinding, these weak interactions can be destroyed and the aromatic rings twist, giving rise to the MCL properties of **HL**·2CH_3CN and complex **1**. Since the conformational twist between TPA phenyl and acceptor groups controlled the solid state fluorescence,[60] the emission of complex **1** is more red-shifted than that of **HL**·2CH_3CN, which may be attributed to the difference in the conformation of the Schiff base molecules and molecular interactions caused by chelation.

Acidochromic properties

Under ambient light, it can be observed that the **HL**·2CH_3CN crystal was pale yellow, and the fluorescence emission position was centered at 464 nm as shown in Fig. 5. When exposed to hydrochloric acid vapor (36% concentrated hydrochloric acid vapor), an obvious color change from pale yellow to orange-red can be easily observed by the naked eye. The orange-red sample was named **HL-HCl**. The emission peak of **HL-HCl** was red-shifted to 594 nm (τ = 0.56 ns), accompanied by the luminescence color change to orange-red. Excitingly, when **HL-HCl** was continued to be fumigated with NH_3 vapor (25% concentrated ammonium hydroxide vapor), named **HL-HCl-NH_3**, the light yellow color under ambient light was restored, with the maximum emission peak blue-shifted to 494 nm (τ = 0.98 ns), and the fluorescence returned to light cyan, which was similar to that of the ground sample. Therefore, **HL**·2CH_3CN exhibited a high-contrast tricolor acidochromic behavior. For complex **1**, after being treated with HCl vapor (36% concentrated hydrochloric acid vapor), the fluorescence emission color changed from cyan to orange, the maximum emission position was red-shifted from 490 to 587 nm (τ = 0.91 ns), and the sample turned orange, which was named **1-HCl**. When **1-HCl** was further fumigated with NH_3 vapor (25% concentrated ammonium hydroxide vapor), the emission peak of the sample (named **1-HCl-NH_3**) reverted to 503 nm (τ = 1.17 ns). Simultaneously, the color under ambient light and the emission color are consistent with the original sample. The above results indicated that complex **1** has reversible and high-contrast acidochromic properties.

PXRD, solid-state UV-vis absorption spectroscopy and X-ray photoelectron spectroscopy (XPS) were carried out to explore the mechanism of the acidochromism of **HL**·2CH_3CN and complex **1**. As shown in Fig. S7,† **HL**·2CH_3CN has strong absorption at 411 nm and weak absorption at 589 nm. The strong absorption peak position of **HL-HCl** is at a longer wavelength than that of **HL**·2CH_3CN (480 nm). Its weak absorption appears at 674 nm. After treatment with NH_3, a similar absorption peak to the original one appeared again. These results can be the reason why the color of **HL-HCl** is different from those of **HL**·2CH_3CN and **HL-HCl-NH_3**. Similarly, complex **1** and **1-HCl** both have strong absorption at 407 nm, while **1-HCl** has new weak absorption peaks at 522 nm and 672 nm, which also leads to the difference in their colors under ambient light.

In order to investigate whether the composition of the surface of the materials has changed, XPS experiments on

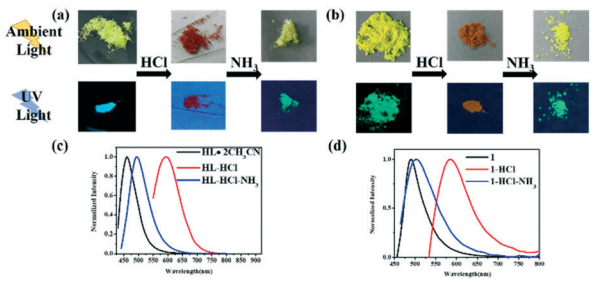

Fig. 5 Images of HL·2CH_3CN (a) and complex **1** (b) in different solid states under ambient light and the irradiation of UV light at 365 nm; emission spectra of HL·2CH_3CN (c) and complex **1** (d) in different solid states.

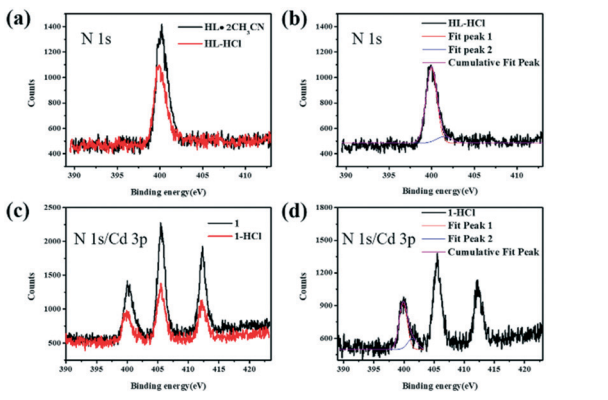

Fig. 6 XPS spectra of HL·2CH_3CN (a) and complex **1** (c) in different states; peak splitting results of **HL-HCl** (b) and **1-HCl** (d).

the original sample and the sample fumigated with HCl vapor were performed (Fig. 6). By comparing the XPS results of **HL**·2CH_3CN with those of **HL-HCl** (Fig. S8†), it can be found that the binding energy of Cl 2p appears at 198.10 eV in **HL-HCl**, but not in **HL**·2CH_3CN, indicating that the elemental composition of **HL-HCl** also contains Cl. In addition, we found that both **HL**·2CH_3CN and **HL-HCl** have a binding energy belonging to N 1s at 400.10 eV, while **HL-HCl** also has a shoulder peak at 402.26 eV belonging to N^+ (Fig. 6d). Meanwhile, there is no difference in the binding energy of O 1s in **HL**·2CH_3CN and **HL-HCl**. Based on the above results, it is speculated that the fumigation with HCl vapor caused the –NH– group of the Schiff base molecules to accept protons from HCl, protonizing into quaternary ammonium salt. The protonation process may cause the HOMO–LUMO energy level of the whole molecule to be perturbed, which causes the color and emission position of the sample to change, making **HL**·2CH_3CN show acidochromic properties. As the structure of the Schiff base molecules in complex **1** was consistent with that in **HL**·2CH_3CN, we can infer that the vapor discoloration of complex **1** is also due to the protonation process of the Schiff base molecules. Undoubtedly, our inference is confirmed by the XPS results of **1** and **1-HCl**. Compared with complex **1**, the binding energy of N^+ also appeared at 402.03 eV in sample **1-HCl**, while the binding energy of O 1s, Cd 3d and Cl 2p showed no significant difference (Fig. S9†). This also showed that the complex is not decomposed under the influence of the HCl vapor.

In order to explore whether the states of the sample have changed after being treated with different vapors, the PXRD results were carefully compared. As shown in Fig. 7a and b, the PXRD pattern of **HL-HCl** showed different diffraction peaks from that of the original sample of **HL**·2CH_3CN indicating that the crystal structure of the original crystal was destroyed, and another crystal structure appeared after protonation. The PXRD pattern of the **HL-HCl-NH$_3$** sample shows a peak attributed to the amorphous state and the characteristic diffraction peak of NH_4Cl at 2θ = 32.76°. Therefore, when the **HL-HCl** sample was further treated with NH_3 vapor, the Schiff base molecules were deprotonated and NH_4Cl was generated, but the original crystalline state was not recovered, which was also confirmed by the consistency of the fluorescence emission of **HL-HCl-NH$_3$** and the ground sample. As shown in Fig. S5,† there is no weight loss for **HL-HCl-NH$_3$** at 60 °C, and its weight loss takes place at 220°, which is lower than that of the ground sample. This may be due to the decomposition of NH_4Cl generated on the surface. Similar to **HL**·2CH_3CN, **1-HCl** also has a different diffraction pattern from the original sample **1**, and the characteristic diffraction peak of NH_4Cl also existed in the PXRD pattern of **1-HCl-NH$_3$**. The emission peak of **1-HCl** can only be restored to 504 nm, which may be related to the incomplete recovery of the original characteristic diffraction peak.

To further understand the acidochromic mechanism of **HL**·2CH_3CN and complex **1**, ^{1}H NMR spectra of the **HL**·2CH_3CN, **HL-HCl**, **HL-HCl-NH$_3$**, **1** and **1-HCl** samples were recorded as shown in Fig. 8. Compared with the ^{1}H NMR spectrum of **HL**·2CH_3CN, there are some new peaks with low intensity which could be ascribed to the proton of reactants 4-(diphenylamino)benzaldehyde and 4-hydroxybenzohydrazide.[61,62] This indicates that the adsorbed HCl leads to the decomposition of **HL** in DMSO. In addition, **HL-HCl** shows a significant upfield shift of the NH proton, indicative of the protonation of the nitrogen on the hydrazide unit. When **HL-HCl** was treated with NH_3, the ^{1}H NMR spectrum resembles that of **HL**·2CH_3CN except the proton signal of NH, indicating the reversible acidochromic behavior. The ^{1}H NMR spectrum of the Cd complex is similar to that of **HL**, confirming that a similar change occurred for complex **1**. Based on the above results, protonation and phase transformation are the reasons for the acid–base responsive behavior of **HL**·2CH_3CN and complex **1**.

Writable and acid stimulus responsive test paper

Based on the high contrast MCL and vapochromic properties of **HL**·2CH_3CN and complex **1**, a simple test paper that can be written on and responds to acid vapor was produced (Fig. 9). The specific process is as follows. The **HL**·2CH_3CN crystals were ultrasonically crushed and dispersed in acetonitrile, then they were added dropwise on a filter paper, and air dried. Due to the small amount of the sample loaded, the test paper was white, but showed strong blue fluorescence under 365 nm irradiation. After that, an "L" character was written on the test paper by using a glass rod. There was no significant change on the test paper under ambient light, but a green-emitting "L" character was seen under UV irradiation. When the test paper was exposed to HCl vapor (36% concentrated hydrochloric acid vapor), its

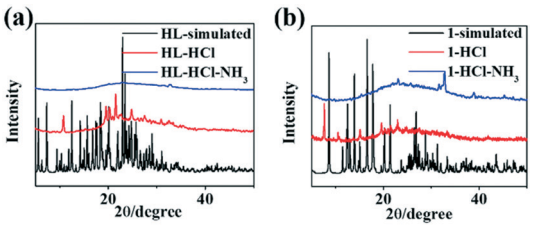

Fig. 7 PXRD patterns of HL·2CH_3CN (a) and complex **1** (b) after different treatments.

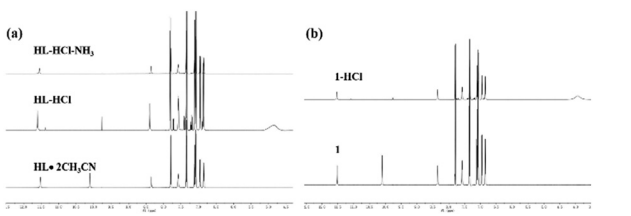

Fig. 8 ^{1}H NMR spectra of HL·2CH_3CN (a) and **1** (b) before and after different treatment in d_6-DMSO.

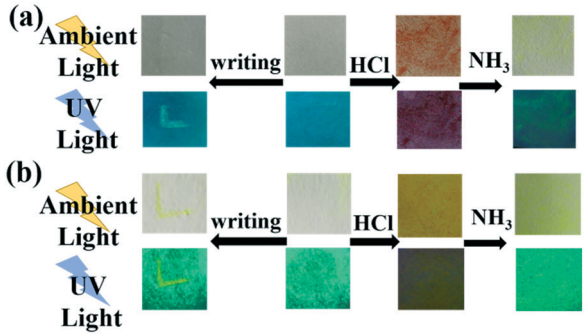

Fig. 9 Photographs of HL·2CH_3CN (a) and complex **1** (b) after different treatments under natural light and 365 nm irradiation.

color changed to red and the fluorescence emission became dark red.

Further treatment with NH_3 vapor (25% concentrated ammonium hydroxide vapor) restored it to yellow and the fluorescence color changed to green. Similarly, a test paper of complex **1** was fabricated. After writing the character "L" on the white test paper with cyan fluorescence using a glass rod, the yellow color with a yellow-emitting character "L" appeared. When treated with HCl vapor, the test paper turned yellow and the fluorescence color turned orange-yellow. The original cyan fluorescence was restored after treatment with NH_3 vapor. Therefore, **HL**·2CH_3CN and complex **1** can be used as writable and acid stimulus responsive materials.

Conclusions

In summary, a triphenylamine derivative and its Cd(II) complex were successfully synthesized by a one-pot reaction. Both compound **HL**·2CH_3CN and complex **1** exhibited high-contrast mechanochromic luminescence and acidochromism. The experimental results showed that the molecules of both **HL**·2CH_3CN and complex **1** possess rich non-covalent interactions, adopting loose packing modes. Therefore, the phase transformation from a crystalline state to an amorphous state can occur effectively, which leads to the mechanochromic luminescence. After treating with organic vapor, the original emission can be restored. In addition, the color and luminescence color of **HL**·2CH_3CN and complex **1** both changed after being exposed to HCl vapor, showing acid–base responsive properties. The results of XPS showed that the protonation of the –NH– group leads to the acidochromic properties. After further treatment with NH_3 vapor, **1-HCl** can be restored to the original state, while **HL-HCl** can only be restored to the same state as the ground sample due to the serious collapse of the original crystal structure and the departure of acetonitrile molecules in the protonation and deprotonation process, thus showing a tricolor acid–base responsive behavior. The research results provide a new strategy for the development of multi-stimulus responsive luminescent materials.

Experimental

Materials and methods

All solvents and reagents in the present work were obtained from commercial sources and used without further purification. The Fourier transform infrared (FT-IR) spectra were recorded on an Avatar 360 FT-IR spectrometer using KBr pellets as an internal standard in 4000–400 cm^{-1}. The ^1H NMR spectra were recorded on a Bruker Avance III 600 MHz spectrometer. The fluorescence quantum yield was measured on a HAMAMATSU Quantaurus-QY instrument. The single crystal X-ray diffraction data were collected with an XtaLAB Synergy-DW and an Oxford Diffraction SuperNova area-detector diffractometer using mirror optics monochromated Cu-Kα radiation (λ = 1.54184 Å) at low temperature (100 K). The X-ray powder diffraction (PXRD) patterns were obtained using a SHIMADZU XRD-7000 diffractometer with Cu-Kα radiation (λ = 1.5418 Å) at 25 °C. The thermogravimetric (TG) data were collected using a Mettler TGA instrument in the range of 30–500 °C under a constant nitrogen flow with a heating rate of 10 K min^{-1}. Differential scanning calorimetry (DSC) was carried out using a Mettler DSC 1 instrument. The solid-state UV-vis absorption spectra were recorded on a TU-1901 spectrophotometer with an integrating sphere at room temperature in the range of 250–800 nm. The X-ray photoelectron spectra (XPS) were obtained by using an ESCALAB 250 Xi spectrometer.

Synthesis

Synthesis of HL·2CH_3CN. 4-(Diphenylamino)benzaldehyde (0.1 mmol, 0.0273 g), 4-hydroxybenzohydrazide (0.1 mmol, 0.0152 g) and 4 mL acetonitrile were added to a closed 25 mL Teflon-lined autoclave and heated at 80 °C for 48 h, and then cooled to room temperature to give a pale yellow clear solution. After the solvent evaporated, yellow crystals of HL·2CH_3CN formed, and were filtered and washed with acetonitrile. Yield: 82.1% (0.0401 g). IR (KBr pellet, cm^{-1}): 3234 s, 1614 *vs.*, 1587 *vs.*, 1572 s, 1508 *vs.*, 1492 s, 1450 w, 1427 m, 1402 m, 1384 w, 1303 s, 1280 *vs.*, 1178 m, 1116 w, 1058 w, 976 w, 846 m, 756 m, 694 s, 592 m. 1H NMR (600 MHz, DMSO-d_6): = 11.52 (s, 1H), 10.10 (s, 1H), 8.35 (s, 1H), 7.79 (d, J = 8.6 Hz, 2H), 7.58 (d, J = 8.3 Hz, 2H), 7.34 (t, J = 7.4 Hz, 4H), 7.11 (t, J = 7.6 Hz, 2H), 7.08 (d, J = 7.4 Hz, 4H), 6.96 (d, J = 8.5 Hz, 2H), 6.85 (d, J = 8.7 Hz, 2H) ppm. Anal. calcd: C, 73.59; N, 14.30; H, 5.55. Found: C, 71.11; N, 12.08; H, 5.15.

Synthesis of Cd(II) complex 1. 4-(Diphenylamino) benzaldehyde (0.1 mmol, 0.0273 g), 4-hydroxybenzohydrazide (0.1 mmol, 0.0152 g), cadmium acetate (0.1 mmol, 0.0230 g), and 4 mL acetonitrile were added to a closed 25 mL Teflon-lined autoclave and heated at 80 °C for 48 h, and then cooled to room temperature. Pale yellow crystals of **1** were obtained, then filtered and washed with acetonitrile. Yield: 57.8% (0.0577 g). IR (KBr pellet, cm^{-1}): 3331 s, 1666 s, 1587 *vs.*, 1491 *vs.*, 1356 m, 1329 m, 1269 s, 1224 m, 1172 s, 1141 m, 1072 w, 952 w, 846 m, 758 m, 698 s, 617 s, 515 m. 1H NMR (600 MHz, DMSO-d_6): = 11.52 (s, 1H), 10.10 (s, 1H), 8.35 (s, 1H),

7.79 (d, J = 8.7 Hz, 2H), 7.58 (d, J = 8.1 Hz, 2H), 7.34(t, J = 7.7 Hz, 4H), 7.11 (t, J = 7.4 Hz, 2H), 7.08 (d, J = 7.6 Hz, 4H), 6.96 (d, J = 8.6 Hz, 2H), 6.85 (d, J = 8.6 Hz, 2H). Anal. calcd: C, 62.56; N, 8.42; H, 4.24. Found: C, 62.39; N, 7.81; H, 4.20.

Conflicts of interest

There are no conflicts to declare.

Acknowledgements

We acknowledge the financial support from the National Natural Science Foundation of China (21671022).

Notes and references

1 X. S. Han, X. Luan, H. F. Su, J. J. Li, S. F. Yuan, Z. Lei, Y. Pei and Q. M. Wang, Structure Determination of Alkynyl-Protected Gold Nanocluster $Au_{22}(^tBu{\equiv}C)_{18}$ and Its Thermochromic Luminescence, *Angew. Chem., Int. Ed.*, 2020, **59**, 2309–2312.

2 X. W. Chen, H. L. Yuan, L. H. He, J. L. Chen, S. J. Liu, H. R. Wen, G. Zhou, J. Y. Wang and W. Y. Wong, A Sublimable Dinuclear Cuprous Complex Showing Selective Luminescence Vapochromism in the Crystalline State, *Inorg. Chem.*, 2019, **58**, 14478–14489.

3 X. Mei, G. Wen, J. Wang, H. Yao, Y. Zhao, Z. Lin and Q. Ling, A Λ-shaped donor–π–acceptor–π–donor molecule with AIEE and CIEE activity and sequential logic gate behaviour, *J. Mater. Chem. C*, 2015, **3**, 7267–7271.

4 D. Kitagawa, T. Nakahama, Y. Nakai and S. Kobatake, 1,2-Diarylbenzene as fast T-type photochromic switch, *J. Mater. Chem. C*, 2019, **7**, 2865–2870.

5 N. A. Simeth, A. C. Kneuttinger, R. Sterner and B. König, Photochromic coenzyme Q derivatives: switching redox potentials with light, *Chem. Sci.*, 2017, **8**, 6474–6483.

6 B. Jiang, J. Zhang, J. Q. Ma, W. Zheng, L. J. Chen, B. Sun, C. Li, B. W. Hu, H. Tan, X. Li and H. B. Yang, Vapochromic Behavior of a Chair-Shaped Supramolecular Metallacycle with Ultra-Stability, *J. Am. Chem. Soc.*, 2016, **138**, 738–741.

7 A. Kobayashi, K. Shimizu, A. Watanabe, Y. Nagao, N. Yoshimura, M. Yoshida and M. Kato, Two-Step Vapochromic Luminescence of Proton-Conductive Coordination Polymers Composed of Ru(II)-Metalloligands and Lanthanide Cations, *Inorg. Chem.*, 2019, **58**, 2413–2421.

8 Y. Wu, X. Zhang, Y. Q. Zhang, M. Yang and Z. N. Chen, Achievement of ligand-field induced thermochromic luminescence via two-step single-crystal to single-crystal transformations, *Chem. Commun.*, 2018, **54**, 13961–13964.

9 K. Mutoh, N. Miyashita, K. Arai and J. Abe, Turn-On Mode Fluorescence Switch by Using Negative Photochromic Imidazole Dimer, *J. Am. Chem. Soc.*, 2019, **141**, 5650–5654.

10 B. Y. W. Wong, H. L. Wong, Y. C. Wong, V. K. M. Au, M. Y. Chan and V. W. W. Yam, Multi-functional bis(alkynyl) gold(iii) N^C complexes with distinct mechanochromic luminescence and electroluminescence properties, *Chem. Sci.*, 2017, **8**, 6936–6946.

11 Y. Matsunaga and J. S. Yang, Multicolor Fluorescence Writing Based on Host–Guest Interactions and Force-Induced Fluorescence-Color Memory, *Angew. Chem., Int. Ed.*, 2015, **54**, 7985–7989.

12 B. Xu, J. He, Y. Mu, Q. Zhu, S. Wu, Y. Wang, Y. Zhang, C. Jin, C. Lo, Z. Chi, A. Lien, S. Liu and J. Xu, Very bright mechanoluminescence and remarkable mechanochromism using a tetraphenylethene derivative with aggregation-induced emission, *Chem. Sci.*, 2015, **6**, 3236–3241.

13 Y. Sagara and T. Kato, Brightly Tricolored Mechanochromic Luminescence from a Single-Luminophore Liquid Crystal: Reversible Writing and Erasing of Images, *Angew. Chem., Int. Ed.*, 2011, **50**, 9128–9132.

14 A. Abdollahi, H. Roghani-Mamaqani, B. Razavi and M. Salami-Kalajahi, Photoluminescent and Chromic Nanomaterials for Anticounterfeiting Technologies: Recent Advances and Future Challenges, *ACS Nano*, 2020, **14**, 14417–14492.

15 K. Y. Zhang, X. Chen, G. Sun, T. Zhang, S. Liu, Q. Zhao and W. Huang, Utilization of Electrochromically Luminescent Transition-Metal Complexes for Erasable Information Recording and Temperature-Related Information Protection, *Adv. Mater.*, 2016, **28**, 7137–7142.

16 T. Ono, Y. Tsukiyama, S. Hatanaka, Y. Sakatsume, T. Ogoshi and Y. Hisaeda, Inclusion crystals as vapochromic chemosensors: fabrication of a mini-sensor array for discrimination of small aromatic molecules based on side-chain engineering of naphthalenediimide derivatives, *J. Mater. Chem. C*, 2019, **7**, 9726–9734.

17 R. Yano, M. Yoshida, T. Tsunenari, A. Sato-Tomita, S. Nozawa, Y. Iida, N. Matsunaga, A. Kobayashi and M. Kato, Vapochromic behaviour of a nickel(ii)-quinonoid complex with dimensional changes between 1D and higher, *Dalton Trans.*, 2021, **50**, 8696–8703.

18 M. Raisch, D. Genovese, N. Zaccheroni, S. B. Schmidt, M. L. Focarete, M. Sommer and C. Gualandi, Highly Sensitive, Anisotropic, and Reversible Stress/Strain-Sensors from Mechanochromic Nanofiber Composites, *Adv. Mater.*, 2018, **30**, 1–6.

19 Y. Pei, J. Xie, D. Cui, S. Liu, G. Li, D. Zhu and Z. Su, A mechanochromic cyclemetalated cationic Ir(iii) complex with AIE activity by strategic modification of ligands, *Dalton Trans.*, 2020, **49**, 13066–13071.

20 X. Zhou, S. Lee, Z. Xu and J. Yoon, Recent Progress on the Development of Chemosensors for Gases, *Chem. Rev.*, 2015, **115**, 7944–8000.

21 H. Sun, S. Liu, W. Lin, K. Y. Zhang, W. Lv, X. Huang, F. Huo, H. Yang, G. Jenkins, Q. Zhao and W. Huang, Smart responsive phosphorescent materials for data recording and security protection, *Nat. Commun.*, 2014, **5**, 2–10.

22 Y. Wang, X. Tan, Y. M. Zhang, S. Zhu, I. Zhang, B. Yu, K. Wang, B. Yang, M. Li, B. Zou and S. X. A. Zhang, Dynamic Behavior of Molecular Switches in Crystal under Pressure and Its Reflection on Tactile Sensing, *J. Am. Chem. Soc.*, 2015, **137**, 931–939.

23 M. Y. Zhang, Q. Peng and C. H. Zhao, High-contrast mechanochromic fluorescence from a highly solid-state

emissive 2-(dimesitylboryl)phenyl-substituted [2.2] paracyclophane, *J. Mater. Chem. C*, 2021, **9**, 1740–1745.

24 B. Hupp, J. Nitsch, T. Schmitt, R. Bertermann, K. Edkins, F. Hirsch, I. Fischer, M. Auth, A. Sperlich and A. Steffen, Stimulus-Triggered Formation of an Anion–Cation Exciplex in Copper(I) Complexes as a Mechanism for Mechanochromic Phosphorescence, *Angew. Chem., Int. Ed.*, 2018, **57**, 13671–13675.

25 D. Qiao, J. Y. Wang, L. Y. Zhang, F. R. Dai and Z. N. Chen, Aggregation-induced emission enhancement and reversible mechanochromic luminescence of quinoline-based zinc(ii)–Schiff base complexes, *Dalton Trans.*, 2019, **48**, 11045–11051.

26 G. Li, Y. Xu, Q. Kong, W. Zhuang and Y. Wang, Cation–anion interaction directed dual-mode switchable mechanochromic luminescence, *J. Mater. Chem. C*, 2017, **5**, 8527–8534.

27 Y. Sagara, K. Takahashi, T. Nakamura and N. Tamaoki, Mechanochromic Luminescence from Crystals Consisting of Intermolecular Hydrogen-Bonded Sheets, *Chem. - Asian J.*, 2020, **15**, 478–482.

28 H. Liu, Y. Gu, Y. Dai, K. Wang, S. Zhang, G. Chen, B. Zou and B. Yang, Pressure-Induced Blue-Shifted and Enhanced Emission: A Cooperative Effect between Aggregation-Induced Emission and Energy-Transfer Suppression, *J. Am. Chem. Soc.*, 2020, **142**, 1153–1158.

29 Q. Nie, Y. Xie, W. Huang and D. Wu, A Dynamic Heterometal–Organic Rhomboid Exhibiting Thermochromic and Piezochromic Luminescence, *Inorg. Chem.*, 2018, **57**, 14489–14492.

30 J. P. Lee, H. Hwang, S. Chae and J. M. Kim, A reversibly mechanochromic conjugated polymer, *Chem. Commun.*, 2019, **55**, 9395–9398.

31 B. Li, L. Cui and C. Li, Macrocycle Co-Crystals Showing Vapochromism to Haloalkanes, *Angew. Chem., Int. Ed.*, 2020, **59**, 22012–22016.

32 W. Yang, Y. Yang, Y. Qiu, X. Cao, Z. Huang, S. Gong and C. Yang, AIE-active multicolor tunable luminogens: simultaneous mechanochromism and acidochromism with high contrast beyond 100 nm, *Mater. Chem. Front.*, 2020, **4**, 2047–2053.

33 A. E. Norton, M. K. Abdolmaleki, J. Liang, M. Sharma, R. Golsby, A. Zoller, J. A. Krause, W. B. Connick and S. Chatterjee, Phase transformation induced mechanochromism in a platinum salt: a tale of two polymorphs, *Chem. Commun.*, 2020, **56**, 10175–10178.

34 D. Peng, L. H. He, P. Ju, J. L. Chen, H. Y. Ye, J. Y. Wang, S. J. Liu and H. R. Wen, Reversible Mechanochromic Luminescence of Tetranuclear Cuprous Complexes, *Inorg. Chem.*, 2020, **59**, 17213–17223.

35 P. Zhang, X. Shi, A. P. H. J. Schenning, G. Zhou and L. T. de Haan, A Patterned Mechanochromic Photonic Polymer for Reversible Image Reveal, *Adv. Mater. Interfaces*, 2020, **7**, 1–7.

36 Y. Pan, H. Zhang, P. Xu, Y. Tian, C. Wang, S. Xiang, R. Boulatov and W. Weng, A Mechanochemical Reaction Cascade for Controlling Load-Strengthening of a Mechanochromic Polymer, *Angew. Chem., Int. Ed.*, 2020, **59**, 21980–21985.

37 X. Wu, J. Guo, Y. Cao, J. Zhao, W. Jia, Y. Chen and D. Jia, Mechanically triggered reversible stepwise tricolor switching and thermochromism of anthracene-o-carborane dyad, *Chem. Sci.*, 2018, **9**, 5270–5277.

38 Y. Zhou, L. Qian, M. Liu, X. Huang, Y. Wang, Y. Cheng, W. Gao, G. Wu and H. Wu, 5-(2,6-Bis((E)-4-(dimethylamino) styryl)-1-ethylpyridin-4(1H)-ylidene)-2,2-dimethyl-1,3-dioxane-4,6-dione: aggregation-induced emission, polymorphism, mechanochromism, and thermochromism, *J. Mater. Chem. C*, 2017, **5**, 9264–9272.

39 Y. Xiong, J. Huang, Y. Liu, B. Xiao, B. Xu, Z. Zhao and B. Z. Tang, High-contrast luminescence dependent on polymorphism and mechanochromism of AIE-active (4-(phenothiazin-10-yl)phenyl)(pyren-1-yl)methanone, *J. Mater. Chem. C*, 2020, **8**, 2460–2466.

40 S. Li, M. Wu, Y. Kang, H. W. Zheng, X. J. Zheng, D. C. Fang and L. P. Jin, Grinding-Triggered Single Crystal-to-Single Crystal Transformation of a Zinc(II) Complex: Mechanochromic Luminescence and Aggregation-Induced Emission Properties, *Inorg. Chem.*, 2019, **58**, 4626–4633.

41 C. Wang and Z. Li, Molecular conformation and packing: their critical roles in the emission performance of mechanochromic fluorescence materials, *Mater. Chem. Front.*, 2017, **1**, 2174–2194.

42 C. Y. Lien, Y. F. Hsu, Y. H. Liu, S. M. Peng, T. Shinmyozu and J. S. Yang, Steric Engineering of Cyclometalated Pt(II) Complexes toward High-Contrast Monomer–Excimer-Based Mechanochromic and Vapochromic Luminescence, *Inorg. Chem.*, 2020, **59**, 11584–11594.

43 Y. Bin Gong, P. Zhang, Y. Rong Gu, J. Q. Wang, M. M. Han, C. Chen, X. J. Zhan, Z. L. Xie, B. Zou, Q. Peng, Z. G. Chi and Z. Li, The Influence of Molecular Packing on the Emissive Behavior of Pyrene Derivatives: Mechanoluminescence and Mechanochromism, *Adv. Opt. Mater.*, 2018, **6**, 1–10.

44 M. Echeverri, C. Ruiz, S. Gámez-Valenzuela, I. Martín, M. C. R. Delgado, E. Gutiérrez-Puebla, M. Á. Monge, L. M. Aguirre-Díaz and B. Gómez-Lor, Untangling the Mechanochromic Properties of Benzothiadiazole-Based Luminescent Polymorphs through Supramolecular Organic Framework Topology, *J. Am. Chem. Soc.*, 2020, **142**, 17147–17155.

45 K. C. Naeem, K. Neenu and V. C. Nair, Effect of Differential Self-Assembly on Mechanochromic Luminescence of Fluorene-Benzothiadiazole-Based Fluorophores, *ACS Omega*, 2017, **2**, 9118–9126.

46 G. Li, T. Yang, K. Shao, Y. Gao, G. Shan, Z. Su, X. Wang and D. Zhu, Understanding Mechanochromic Luminescence on Account of Molecular Level Based on Phosphorescent Iridium(III) Complex Isomers, *Inorg. Chem.*, 2021, **60**, 3741–3748.

47 S. Yokomori, S. Dekura, T. Fujino, M. Kawamura, T. Ozaki and H. Mori, Vapochromism induced by intermolecular electron transfer coupled with hydrogen-bond formation in zinc dithiolene complex, *J. Mater. Chem. C*, 2020, **8**, 14939–14947.

48 E. Li, K. Jie, M. Liu, X. Sheng, W. Zhu and F. Huang, Vapochromic crystals: understanding vapochromism from

the perspective of crystal engineering, *Chem. Soc. Rev.*, 2020, **49**, 1517–1544.

49 K. Wada, T. Kakuta, T. A. Yamagishi and T. Ogoshi, Obvious vapochromic color changes of a pillar[6]arene containing one benzoquinone unit with a mechanochromic change before vapor exposure, *Chem. Commun.*, 2020, **56**, 4344–4347.

50 R. Goswami, S. Das, N. Seal, B. Pathak and S. Neogi, High-Performance Water Harvester Framework for Triphasic and Synchronous Detection of Assorted Organotoxins with Site-Memory-Reliant Security Encryption via pH-Triggered Fluoroswitching, *ACS Appl. Mater. Interfaces*, 2021, **13**, 34012–34026.

51 P. S. Hariharan, E. M. Mothi, D. Moon and S. P. Anthony, Halochromic Isoquinoline with Mechanochromic Triphenylamine: Smart Fluorescent Material for Rewritable and Self-Erasable Fluorescent Platform, *ACS Appl. Mater. Interfaces*, 2016, **8**, 33034–33042.

52 P. Pallavi, V. Kumar, M. D. W. Hussain and A. Patra, Excited-State Intramolecular Proton Transfer-Based Multifunctional Solid-State Emitter: A Fluorescent Platform with "Write-Erase-Write" Function Pragyan, *ACS Appl. Mater. Interfaces*, 2018, **10**, 44696–44705.

53 Z. H. Guo, Z. X. Jin, J. Y. Wang and J. Pei, A donor–acceptor–donor conjugated molecule: twist intramolecular charge transfer and piezochromic luminescent properties, *Chem. Commun.*, 2014, **50**, 6088–6090.

54 Z. Ning, Z. Chen, Q. Zhang, Y. Yan, S. Qian, Y. Cao and H. Tian, Aggregation-induced Emission (AIE)-active Starburst Triarylamine Fluorophores as Potential Non-doped Red Emitters for Organic Light-emitting Diodes and Cl2 Gas Chemodosimeter, *Adv. Funct. Mater.*, 2007, **17**, 3799–3807.

55 M. H. Barbee, K. Mondal, J. Z. Deng, V. Bharambe, T. V. Neumann, J. J. Adams, N. Boechler, M. D. Dickey and S. L. Craig, Mechanochromic Stretchable Electronics, *ACS Appl. Mater. Interfaces*, 2018, **10**, 29918–29924.

56 Y. Gong, J. Liu, Y. Zhang, G. He, Y. Lu, W. Bin Fan, W. Z. Yuan, J. Z. Sun and Y. Zhang, AIE-active, highly thermally and morphologically stable, mechanochromic and efficient solid emitters for low color temperature OLEDs, *J. Mater. Chem. C*, 2014, **2**, 7552–7560.

57 Y. Zhang, Y. Q. Feng, J. H. Wang, G. Han, M. Y. Li, Y. Xiao and Z. D. Feng, Moiety effect on the luminescent property of star-shaped triphenylamine (TPA) derivatives as mechanochromic materials, *RSC Adv.*, 2017, **7**, 35672–35680.

58 P. S. Hariharan, E. M. Mothi, D. Moon and S. P. Anthony, Halochromic Isoquinoline with Mechanochromic Triphenylamine: Smart Fluorescent Material for Rewritable and Self-Erasable Fluorescent Platform, *ACS Appl. Mater. Interfaces*, 2016, **8**, 33034–33042.

59 B. Huang, D. Jiang, Y. Feng, W. C. Chen, Y. Zhang, C. Cao, D. Shen, Y. Ji, C. Wang and C. S. Lee, Mechanochromic luminescence and color-tunable light-emitting devices of triphenylamine functionalized benzo[d,e]benzo[4,5]imidazo[2,1-a]isoquinolin-7-one, *J. Mater. Chem. C*, 2019, **7**, 9808–9812.

60 P. Gayathri, M. Pannipara, A. G. Al-Sehemi and S. P. Anthony, Triphenylamine-based stimuli-responsive solid state fluorescent materials, *New J. Chem.*, 2020, **44**, 8680–8696.

61 L. Mugherli, O. N. Burchak, L. A. Balakireva, A. Thomas, F. Châtelain and M. Y. Balakirev, In Situ Assembly and Screening of Enzyme Inhibitors with Surface-Tension Microarrays, *Angew. Chem., Int. Ed.*, 2009, **48**, 7639–7644.

62 J. Zhang, G. Wu, C. He, D. Deng and Y. Li, Triphenylamine-containing D–A–D molecules with (dicyanomethylene)pyran as an acceptor unit for bulk-heterojunction organic solar cells, *J. Mater. Chem.*, 2011, **21**, 3768–3774.